River Flow 2010 - Dittrich, Koll, Aberle & Geisenhainer (eds) © 2010 Bundesanstalt für Wasserbau ISBN 978-3-939230-00-7

Influence of macro-rough banks on steady flow in a channel

T. Meile
HydroCosmos SA, Grand-Rue 43, 1904 Vernayaz, Switzerland

J.-L. Boillat & A. J. Schleiss
Laboratory of Hydraulic Constructions, Ecole Polytechnique Fédérale de Lausanne, 1015 Lausanne, Switzerland

ABSTRACT: High-head storage hydropower plants operate their turbines during periods of high energy demand. The starting and stopping of turbines results in rapid fluctuations of discharge and water levels in rivers called hydropeaking, which are unfavorable from an ecological point of view. Morphological measures might help to reduce the fluctuations by increasing the natural retention capacity of rivers. With this practical background, the experimental investigations presented in this paper focused on the determination of the flow resistance under steady flow conditions caused by large scale roughness elements at the channel banks, namely rectangular cavities (depressions). The experiments conducted in 41 different geometrical configurations showed various two dimensional flow characteristics in the cavities. The overall head-loss of the flow is governed by the existence of different phenomena such as vertical mixing layers, wake-zones, recirculation gyres, coherent structures and skin friction. The analysis of the experiments for steady flow conditions showed that the flow resistance is significantly increased in the macro-rough configurations due to the disturbance of the bank geometry. Three different approaches have been considered relating the additional flow resistance due to macro-roughness to the forms of the banks. By separating the observed flow conditions into a square grooved, a reattachment and a normal recirculating flow type, the developed macro-rough flow resistance formulas are in good agreement with the laboratory experiments. Furthermore, water body oscillations have been observed in axi-symmetric macro-rough configurations. They lead to water-surface oscillations and transverse velocity components.

Keywords: Macro-roughness, Flow resistance, Cavity flow, Steady channel flow

1 INTRODUCTION

High-head storage hydropower plants operate their turbines during periods of high energy demand. The starting and stopping of turbines result in rapid and frequent fluctuations of discharge and water levels in rivers, called hydropeaking, which are unfavorable from an ecological point of view.

Literature reviews on the effects of hydropeaking (e.g. Baumann and Klaus 2003, Cushman 1985) report the stranding of macro-invertebrates due to rapid ramping or an increase of catastrophic drift (e.g. Céréghino et al. 2002) during sudden increases in discharge, water levels and flow velocities. Morphological measures might help to reduce the fluctuations further downstream by increasing the natural retention capacity since the propagation and attenuation of the (surge) waves are influenced by the channel slope and roughness (Favre 1935) as well as the river morphology (passive retention, Stranner 1996).

With this practical background, experimental investigations have been conducted in a large number of different geometrical configurations, namely rectangular cavities at the river banks. The steady flow experiments consisted in a preliminary step for unsteady flow experiments (Meile 2007, Meile et al. 2008). They focused on the determination of the flow resistance and flow conditions caused by large scale roughness elements (rectangular cavities) at the channel banks.

2 THEORETICAL CONSIDERATIONS

2.1 *Macro-rough flows*

Flows might be classified regarding the effect of the viscosity relative to the inertia in laminar, tur-

bulent and transitional flows. The turbulent flows can again be divided into three types: smooth turbulent flows, fully rough turbulent flows and transitional turbulent flows.
When the relative roughness becomes high, which means that the size of roughness elements approaches the order of magnitude of the flow depth h or the hydraulic radius R_h, the flow is called macro-rough. The roughness elements can cover the entire channel section or only a part of the section as the bottom or the bank. The roughness generating elements may are boulders or pebbles, artificial elements as cubes, spheres, cones or depressions, different types of vegetation, bed forms in mountain streams and torrents, bed forms in mid- and lowland streams or abrupt changes of channel sections respectively profile.

Table 1. Flow types and head-loss governing phenomena.

Flow type		Head-loss due to
Laminar flow ($Re = 4UR_h / \nu < 2300$)		Viscous friction
Transitional flow ($2300 < \mathrm{Re} < 4500$)		Viscous and turbulent friction
Turbulent flow	Smooth turbulent flow	Turbulent friction in the shear layer; no influence of ε
	Transitional turbulent flow	Turbulent friction in the shear layer (influence of Re and ε)
	Fully rough turbulent flow	Turbulent friction in the shear layer; no influence of Re
Macro-rough flow	Well inundated flow	Principally turbulent friction in the shear layer
	Marginally inundated flow	Turbulent friction in the shear layer & wake dissipation
	Partially inundated flow	Principally jet dissipation and wake dissipation

Macro-rough flows have only marginally been studied before 1970. The first systematic investigations on macro-roughness in open channel flow have been done by Bathurst (1978) and on roughness elements in pipe flow by Morris (1955). A further separation of the macro-rough flow can be undertaken using the definitions of Lawrence (1997) into well inundated flow regimes, marginally inundated flow regimes and partially inundated flow regimes (Table 1). Weichert (2006) reviewed flow resistance formulas in mountain streams including macro-rough flows. He divided flow resistance formulas into logarithmic laws with modified constants, modified logarithmic laws, power laws, and laws for macro-and meso-scale features (e.g. Ferro 2003, Wang Zhao-Yin et al., 2009).

An important and general finding of the various studies on macro rough flow resistance is the fact that high roughness density does not automatically mean high flow resistance. Particular arrangements can lead to maximum flow resistance. This has been confirmed by recent studies on boulders and pebbles (Canovaro and Solari 2006, Pagliara and Chiavaccini 2006) even for numerical simulations of artificially roughened beds (Leonardi et. al 2003).

2.2 *Composite and compound channel sections*

The flow resistance and thus water levels of rivers are influenced by the roughness of the bed and the roughness of the banks. For low relative flow depths the roughness of the banks is of secondary importance. This is generally the case for wide rivers at low and moderate discharge.

With increasing relative flow depths, the influence of bank roughness becomes more significant. Different equations issuing from various researches for composite channel resistance exist. They are based on numerous assumptions summarized in Yen (2002). Most of them require an assumption on how the composite/compound channel section is divided. Few others are free of this assumption (Einstein 1934). The concept of the approach of Einstein (1934) is based on the assumption that the total cross sectional mean velocity U is equal to each sub-area mean velocity U_i. The composite Manning coefficient n_c of the section calculates than as:

$$n_c = \left[\frac{1}{P} \sum \left(n_i^{3/2} P_i \right) \right]^{2/3} \quad (1)$$

where P = wetted perimeter, n_i = the Manning coeffient of the sub-area and P_i = wetted perimeter of the sub-area.

The uniform cross sectional velocity hypothesis (single channel method SCM) assumption is quite reasonable for a channel section of composite roughness. However, it becomes more doubtful for a compound channel having a main channel and floodplain(s) where the flow velocities are obviously different from the main channel flow velocity. In this case, the section is divided into subsections and the discharge is computed in each individually (divided channel method DCM). Furthermore, the turbulent exchange (momentum flux due to the velocity gradient)and the geometrical transfer (discharge flux due to geometrical changes of the floodplain) should be taken into account (e.g. Bousmar and Zech 1999).

2.3 *Skin friction and form drag*

In addition to the effect of bed and bank, the total resistance in a channel is depending on both, grain

roughness and form roughness, for example generated by the bed forms of alluvial channels.

For the flow in rough conduits, Morris (1955) applied a concept based on skin friction, caused by the roughness of the material, and form drag. A first friction factor for smooth-turbulences corresponding to walls without macro-scale roughness and a second friction factor caused by roughness elements are considered. The importance of the second friction factor depends on size, form and spacing of the roughness elements

The skin friction is generally described by the concept of bed shear stress (logarithmic formulas) whereas the form resistance is expressed by the balance between hydrodynamic and resistance forces. For the practical description of flow resistance it is often suitable to attribute the spill resistance (wake interference) and free surface distortion also to the form drag (Weichert 2006). The total friction coefficient is:

$$f_{total} = f_{grain} + f_{form} \tag{2}$$

where f_{total} corresponds to the overall friction coefficient, f_{grain} to the skin friction coefficient of the rough channel bed and f_{form} to the friction due to bed forms.

This equation is based on the total shear stress $\tau_0 = \rho g R_h S_0$ and the decomposition of the slope into two components (Meyer-Peter and Müller 1948). It is important to distinguish the composite resistance concept describing the contribution of different phenomenon of a reach (skin friction, form drag) from the composite resistance for a section having different wall characteristics (same phenomenon, different roughness).

In the present experimental study, comparing the friction of a prismatic channel to a channel including macro-roughness at the channel side walls (large scale depression roughness leading to form resistance), the concept above will be used as follows:

$$f_m = f_{prism} + f_{MR} \tag{3}$$

where f_m corresponds to the overall friction. f_{prism} includes all effects contributing to the friction of the prismatic channel but without the macro-roughness elements. f_{MR} accounts for the additional friction due to the macro-rough channel side walls.

3 STEADY FLOW EXPERIMENTS

3.1 *Test flume*

The hydraulic model tests have been performed in a flume with a useful length of 38.33 m and a mean bed slope of 1.14 ‰ (Fig. 1, Fig. 2). The channel is divided from upstream to downstream into an inlet reach (length 7.41 m), a reach with large scale depression roughness at the banks (26.92 m) and an outlet reach (4.0 m). The channel bottom is made of painted steel. The sidewalls of the inlet reach are constructed by wooden boards. The sidewalls of the reach including the large scale depressions, namely rectangular cavities, and the outlet reach are formed by smooth limestone bricks. The channel bed is fix and no sediment transport is taken into account.

A particularly shaped cross section was placed at the downstream end of the outlet reach. Its geometry was optimized in order to reproduce uniform flow conditions along the prismatic channel without macro-roughness. Flow conditions were subcritical during the tests due to the small slope and the section at the outlet for the range of desired discharges. The geometry of the section has been optimized using an approach proposed by Carlier (1988).

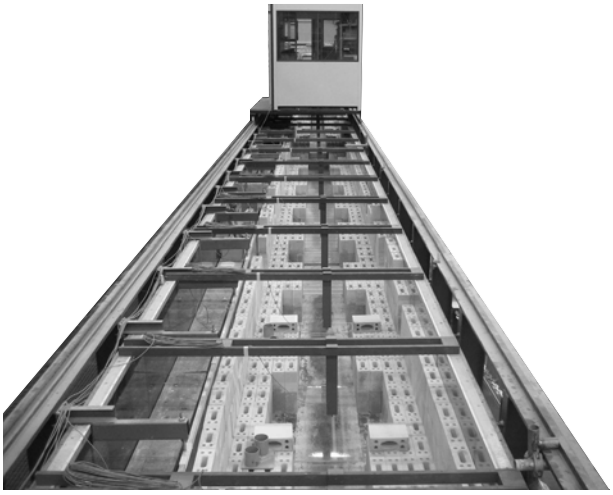

Figure 1. Test flume of the Laboratory of Hydraulic Constructions LCH at EPFL.

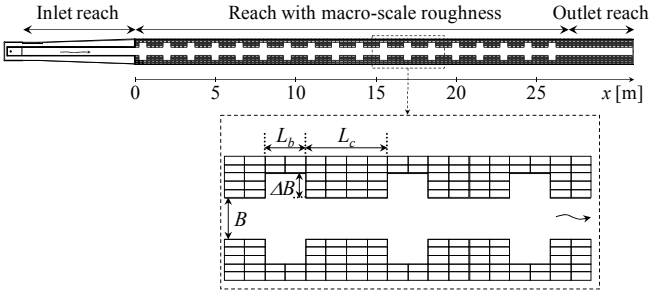

Figure 2: Situation of the test flume. Variable parameters of the macro-rough configurations are L_b, L_c and ΔB.

3.2 *Test geometries*

The channel base width is B = 0.485 ± 0.002 m and remained constant during all the tests. The macro-roughness elements considered in this research are large scale depression roughness (Morris 1955) at both channel banks. Three geometric-

al parameters namely the length of the cavity L_b, the distance between two cavities L_c and the lateral extent of the cavities ΔB, are systematically varied (Fig. 2). Table 2 summarizes the range of the investigated geometrical parameters L_b, L_c and ΔB. The aspect and expansion ratios of the cavity are defined as $AR = \Delta B / L_b$ and $ER = (B + 2\Delta B) / B$ respectively. The combination of three different values for L_b and L_c and four different values of ΔB results in the 36 different, axi-symmetric geometrical configurations covering 8 aspect and 4 expansion ratios. Additionally, 3 of the 36 axi-symmetric configurations have been tested in an asymmetric arrangement and a randomly generated configuration has also been analyzed.

Table 2. Summary of test range of geometrical parameters

Cavity length L_b	0.5 m, 1.0 m, 2.0 m
Distance between cavities L_c	0.5 m, 1.0 m, 2.0 m
Lateral extent of the cavity ΔB	0.1 m, 0.2 m, 0.3 m, 0.4 m
Aspect ratios $\Delta B / L_b$	0.05, 0.10, 0.15, 0.20, 0.30, 0.40, 0.60, 0.80
Expansion ratios $(B+2\Delta B) / B$	1.41, 1.82, 2.24, 2.65

The equivalent sand roughness of the limestone bricks without macro-roughness has been determined by means of backwater curve computations in prismatic reference configuration. Friction coefficients have been calculated using the logarithmic law with the constants of Rouse (1965). The equivalent sand roughness of the wall and the bottom are k_{sw}=0.021 mm and k_{s0}=0.001 mm respectively. The channel bed made of smooth painted steel is fix without sediment transport.

3.3 *Measurements and recordings*

The discharge during the tests was controlled by an electromagnetic flow meter. The water levels have been recorded with ultrasonic elevation probes located along the channel axis (Fig. 1, Fig. 2). The accuracy of the measurements is at least ± 0.002 m. Characteristic values of $Fr = U \cdot (g \cdot h)^{-1}$ (Froude number) and $Re = U \cdot R_h \cdot \nu^{-1}$ (Reynolds number) relative to the base width B ranged between $0.37 < Fr < 0.64$ and $6'800 < Re < 110'000$ for typical flow depths between $0.03\ \text{m} < h < 0.34\ \text{m}$ and mean flow velocities between $0.24\ \text{ms}^{-1} < U < 0.80\ \text{ms}^{-1}$. U is the mean flow velocity in the cross-section and R_h is the hydraulic radius, both calculated relative to the small channel section at base width B.

4 RESULTS

The observations of the flow pattern as well as the water level and the velocity measurements in a channel with macro-roughness elements at the banks show that the flow has steady characteristics from a time-averaged point of view. Nevertheless, the flow characteristics are highly unsteady if instantaneous patterns are considered. They result from the superposition of several complex phenomena such as recirculation gyres, coherent structures, vertical mixing layers, wake-zones and transverse oscillations of the flow (Fig.3).

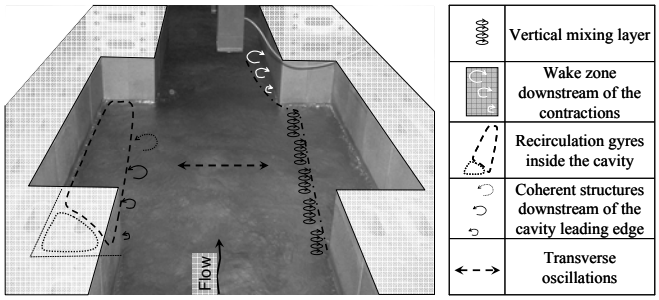

Figure 3: Schematic representation of the different phenomena observed in the channel with macro-rough banks.

Transverse oscillations have been found to be particular significant around Strouhal numbers $St = f \cdot L_b / U$ of 0.42, 0.84 and 1.26 (Meile et al. 2010 (submitted)), where f is the Eigenfrequency of the first mode of sloshing of the waterbody contained in the widened channel part (width $W = B + 2\Delta B$) transverse to the main flow.

Principally three different flow types in the depressions can be distinguished: the reattachment flow type, the normal recirculating flow type and the square grooved flow type (Fig. 4). For some exceptions, namely low velocity flows, flow remains recirculating also in cavities with ratios $h/B \leq 0.1$ (Meile 2007, Weitbrecht 2004).

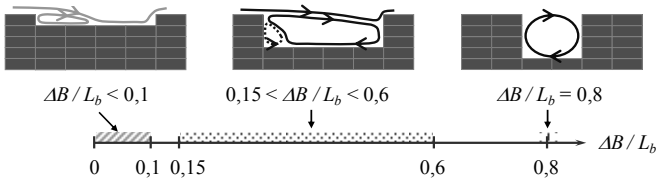

Figure 4: Observed basic flow types in the large-scale depressions.

Not all of the mentioned phenomena of Fig. 3 exist with the same relative importance in all geometrical configurations. However, all active phenomena contribute to the total head-loss along the macro-rough channel. In the following chapters (§ 4.1 and § 4.2), the flow resistance of the investigated configurations, including all effects of the above mentioned phenomena, will be identified and macro-rough flow resistance laws are developed.

4.1 *Analysis of the flow resistance*

Systematic comparison of the different macro-rough configurations requires the identification of roughness parameters. They have been derived from backwater curve computations starting from downstream and using the standard step method.

In a first step, the bottom and wall roughness of the prismatic configuration were determined for 10 different discharges by minimizing the last square errors between measured and calculated flow depths ("inverse roughness modelling", Sieben 2003. When macro-roughness elements are considered, the flow is still uniform in the prismatic outlet reach of the channel, but a backwater curve starts at the downstream end of the macro-rough reach.

The backwater curve computation is based on a one dimensional prismatic approach, even if the channel banks include large-scale roughness. The friction slope S_f is calculated by the Darcy-Weisbach formula:

$$\overline{S_{fm}} = \overline{f_m}\,\frac{\overline{U}^2}{8g\,\overline{R_h}} \tag{4}$$

where R_h = hydraulic radius; f = friction coefficient. The horizontal bar indicates that averaged values between sections i and $i + 1$ are taken into account. The subscript m refers to the composite section.

The channel section has been considered having composite roughness. Using the assumption of the approach of Einstein (1934) for a section of composite roughness, one can write:

$$\frac{R_{h0}}{f_0} = \frac{R_{hw}}{f_w} = \frac{R_{hm}}{f_m} = \frac{U^2}{8gS_{fm}} \tag{5}$$

where R_{h0} = hydraulic radius referred to the bottom; R_{hw} = hydraulic radius referred to the wall; R_{hm} = hydraulic radius referred to the section at base width B.

The composite friction coefficient of the section f_m is calculated according to Eq. (6). The formula is derived from the Darcy-Weisbach formula using Einstein's approach for composite channel sections.

$$f_m = \frac{B f_0 + 2h f_w}{B + 2h} \tag{6}$$

where f_0 = bottom friction coefficient; f_w = wall friction coefficient including the effect of macro-roughness of the widenings.

The bottom and wall friction coefficients are determined iteratively with logarithmic laws:

$$\frac{1}{\sqrt{f_0}} = -K_1 \log\left(\frac{k_{s0}}{K_2\,R_{h0}} + \frac{K_3}{4Re_0\sqrt{f_0}}\right) \tag{7a}$$

$$\frac{1}{\sqrt{f_w}} = -K_1 \log\left(\frac{k_{sw}}{K_2\,R_{hw}} + \frac{K_3}{4Re_w\sqrt{f_w}}\right) \tag{7b}$$

where Re_0 = Reynolds number related to the bottom; Re_w = Reynolds number related to the wall; $k_{s,0}$ = equivalent bottom sand roughness; $k_{s,w}$ = equivalent wall sand roughness including the effect of macro-roughness of widenings. $K_1 = 2.03$, $K_2 = 10.95$ and $K_3 = 1.70$ are the constants utilized by Rouse (1965). Backwater curve computations for the prismatic channel showed good agreement with the hydraulic behaviour of the laboratory flume by using these constants.

The hydraulic radius R_{h0}, R_{hw}, and the Reynolds numbers Re_0 and Re_w are calculated as:

$$R_{h0} = \frac{R_{hm}}{f_m} f_0 \quad \text{(8a)} \qquad R_{hw} = \frac{R_{hm}}{f_m} f_w \quad \text{(8b)}$$

$$Re_0 = \frac{U\,R_{h0}}{\nu} \quad \text{(9a)} \qquad Re_w = \frac{U\,R_{hw}}{\nu} \quad \text{(9b)}$$

The f_m-values of the composite section can be found by this approach for all configurations and discharges. The values are almost independent on the hypothesis made by the introduction of Eq. (5) to (9) and nearly constant along the channel for a given discharge and a given macro-rough configuration. Furthermore, the wall friction coefficients f_w including the effect of macro-roughness could be extracted.

The dataset of f_m values is used to develop macro-rough flow resistance formulas according the principal of decomposition of the total flow resistance according Eq. (3) into a prismatic and a macro-rough part exemplarily shown in Fig. 5.

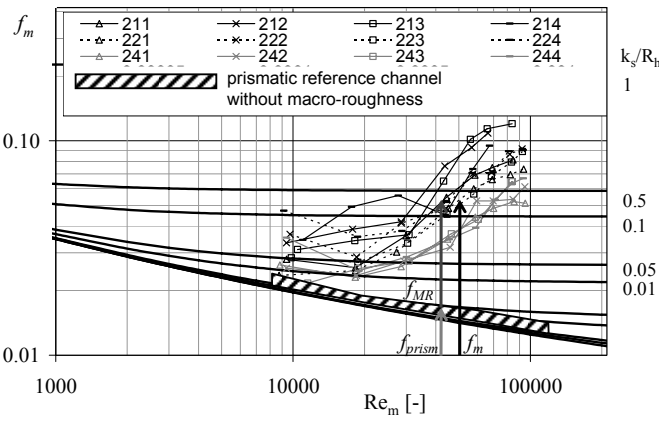

Figure 5: Friction coefficient of the composite channel section f_m (including MR) illustrated for configurations 211 to 244 as a function of the Reynolds number Re_m.

4.2 *Computation of the macro-rough flow*

In this chapter two different approaches are used in order to propose macro-rough flow resistance formulas for macro-roughness at channel banks. The first approach is based on the dimensionless analysis (power-law optimization). The second approach results in a semi-empirical formula which is physically based on a drag coefficient model. A third approach uses Evolutionary Polynomial Regression (Giustolisi and Savic 2006). It is described in Meile (2007).

A)Power-law optimization

Analogous to the dimensional analysis of the pipe flow problem it can be written:

$$\frac{\Delta p}{\Delta l} = \xi\ R_h^{\ a}\ B^b\ \Delta B^c\ L_b^{\ d}\ L_c^{\ e}\ U^f\ \rho^g\ \mu^h\ k_s^{\ i} \qquad (10)$$

The variables R_h, U, ρ, μ, k_s are well known from dimensional analysis of the pipe flow whereas the variables B, ΔB, L_b, L_c are specific to the macro-rough configurations. ξ is a constant. $\Delta pU/\Delta l$ is the pressure drop par unit length.

The final result of the dimensional analysis is similar to a friction coefficient when dividing formula Eq. (10) by $\xi(U^2\rho / R_h)$ and choosing $\xi = 1/8$.

$$f_m = \frac{h_r}{\Delta l}\frac{2g}{U^2}4R_h = f\left(\frac{B}{R_h};\frac{\Delta B}{R_h};\frac{L_b}{R_h};\frac{L_c}{R_h};\mathrm{Re}_m;\frac{k_s}{R_h}\right) \qquad (11)$$

Thus, the total friction-loss depends on the Reynolds number and the relative roughness (skin friction) as well as the dimensionless characteristics of the macro-rough configurations.

Since friction coefficients can be summed up, it is possible to split the coefficient f_m into a friction coefficient due to the macro-roughness elements and a friction coefficient due to the skin friction. Parameters related to the macro-rough configurations appear only in the f_{MR}-coefficient. The relative roughness k_s/R_h of the prismatic channel without macro-roughness appears in the f_{prism}-coefficient which corresponds to the friction coefficient observed in the prismatic channel. It accounts for the bottom and wall roughness but not for the macro-roughness.

$$f_{MR} = f\left(\frac{B}{R_h};\frac{\Delta B}{R_h};\frac{L_b}{R_h};\frac{L_c}{R_h};\mathrm{Re}_m\right) \qquad (12)$$

$$f_{prism.} = f\left(\mathrm{Re}_m;\frac{k_s}{R_h}\right) \qquad (13)$$

In addition to the dimensionless parameters found by means of Eq. (10), some parameters issued from Morris' approach (Morris 1955) have been added, namely the relative roughness spacing $(L_b + L_c) / R_{hm}$ and a parameter including all cavity characteristics $(L_b + L_c) / \Delta B$.

For the square grooved, reattachment and normal recirculating flow types (Fig. 4), and after pre-selection of the parameters using the Pearson product-moment correlation, flow resistance formula of the following type can be determined:

$$C_{adim,MR} = \sqrt{\frac{8}{f_{MR}}} = \xi \cdot A^{\alpha} \cdot B^{\beta} \cdot C^{\gamma} \ldots \qquad (14)$$

where A, B, C … are dimensionless parameters and α, β, γ, … the exponents of the power law. ξ is a constant. $C_{adim,MR}$ is the dimensionless, macro-rough Chezy coefficient. The resulting formulas are for the **s**quare **g**rooved (subscript *sg*) flow type:

$$C_{adim\ MR,sg} = \sqrt{\frac{8}{f_{MR,sg}}} = 5 \cdot \left(\frac{L_b + L_c}{R_{hm}}\right)^{1/3} \qquad (15)$$

For the reattachement flow type (subscript *re*):

$$C_{adim\ MR,re} = \sqrt{\frac{8}{f_{MR,re}}} = \left(\frac{L_b + L_c}{\Delta B}\right)^{0.43}\left(\frac{B}{R_{hm}}\right)^{0.9} \qquad (16)$$

For the normal recirculating flow type (subscript *nc*):

$$C_{adim\ MR,nc} = \sqrt{\frac{8}{f_{MR,nc}}} = \left(\frac{L_b + L_c}{\Delta B}\right)^{0.43} \cdot \left[\log(\mathrm{Re}_m)\right]^{0.24} \cdot \left(\frac{B}{R_{hm}}\right)^{0.9} \qquad (17)$$

The resistance formula for the square grooved flow type depends only on the constant $\zeta = 5$ and the relative roughness spacing $(L_b + L_c) / R_{hm}$. This dimensionless parameter has also been identified as the main parameter influencing the flow resistance by Morris (1955) for the skimming flow case.

For the reattachment flow type, the constant becomes ζ=1. The first dimensionless term describes the cavity characteristics and has an exponent of 0.43. The second term takes into account the cross section geometry (exponent of 0.9).

The empirical resistance formula for the normal recirculating flow type, is similar to the reattachment flow type. Nevertheless, the turbulence characteristics $\log(\mathrm{Re}_m)$ of the flow are taken into account with an exponent of 0.24. Due to the high scattering, this formula has limited applicability.

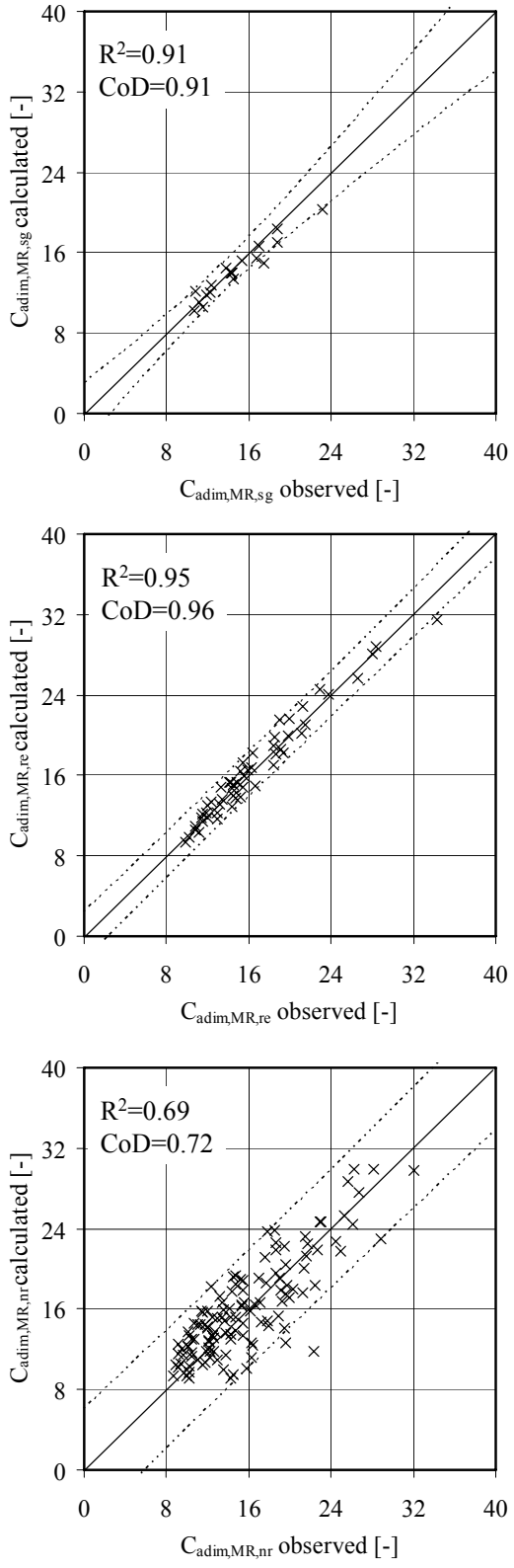

Figure 6: Friction coefficients from empirical formulas based on the Power-law optimization. R^2: correlation coefficient. CoD: coefficient of determination (also Nash coefficient). - - - -: 95% confidence bound.

B)Semi-empirical drag coefficient model

The basic idea for the physically based drag force model is inspired by the partially inundated flow concept of Lawrence (1997) and the work of Morris (1955) on roughened pipes. The definitions used for the mathematical model are shown in Fig. 7.

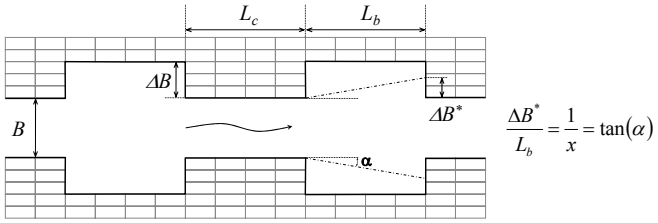

Figure 7: Parameters of the drag force model.

The drag force formula can be written as:

$$F_r = C_d A_r \rho \frac{U^2}{2} = \Delta p A \tag{18}$$

where F_r is the drag force, C_d the drag coefficient, A_r the area on which the drag acts, U the mean velocity in the main channel at base width B, Δp the pressure drop and A the flow surface in the main channel. When replacing the pressure drop $\Delta p = \gamma \cdot h_r$ and $h_r = S_{f,MR}\Delta x = S_{f,MR}(L_b + L_c)$ one obtains:

$$C_d A_r \frac{U^2}{2g} = S_{f,MR}(L_b + L_c)A \tag{19}$$

In this formula, the macro-rough friction slope is replaced by $S_{f\text{-}MR} = f_{MR} \cdot U^2/(8g \cdot R_{hm})$. (19) becomes:

$$C_d A_r = f_{MR} \frac{1}{4R_{hm}}(L_b + L_c)A \tag{20}$$

where $A = B \cdot h$ and $A_r = 2\Delta B^* \cdot h$. Finally, the macro-rough friction coefficient becomes:

$$f_{MR} = C_d \frac{8R_{hm}\Delta B^*}{B(L_b + L_c)} \tag{21}$$

$$\Delta B^* = \min(\Delta B; L_b / x) \tag{22}$$

ΔB^* is the minimum value of the geometric cavity depth and an effective cavity depth considering a certain expansion of the flow ($1/x$) inside of the cavity (Fig. 7).

For the reattachment flow type, ΔB^* becomes equal to ΔB and the experimentally determined drag coefficient $C_d = 0.475$. For the normal recirculating flow type, the same C_d coefficient of 0.475 can be used. The value of x was not found constant but depends on the Reynolds number and the aspect ratio of the cavity. x can be expressed by the following, fully empirical formula:

$$x = \left(\frac{\mathrm{Re}_{\lim}}{\mathrm{Re}_m} + x_0\right)\left(\frac{L_b}{\Delta B}\right)^{0.18} \tag{23}$$

where $Re_{lim} = 150'000$ and $x_0 = 4.5$. The above presented mathematical approach has been applied to reattachment and normal recirculating flow types. For the square grooved flow type at

relatively high Reynolds numbers the macro-rough friction coefficients are calculated according to the skimming flow approach from Morris (1955). The formula is based on the energy required to maintain the rotation of the gyre in the groove of a pipe. It has been adapted for the present experimental study dealing with macro-roughness elements at the side walls as:

$$f_{MR,sg} = \left(\frac{2h}{B+2h}\right)^{\alpha} \cdot \left(\frac{L_b}{L_b+L_c}\right)^{\beta} \cdot \left(\frac{c_w \cdot V_w}{U}\right)^{3} \quad (24)$$

where $\alpha = 0.525$, $\beta = 0.75$, $V_w / U = 2/3$ and $c_w = 0.85$. Fig. 8 to 10 compares calculated and observed macro-rough Chezy coefficients.

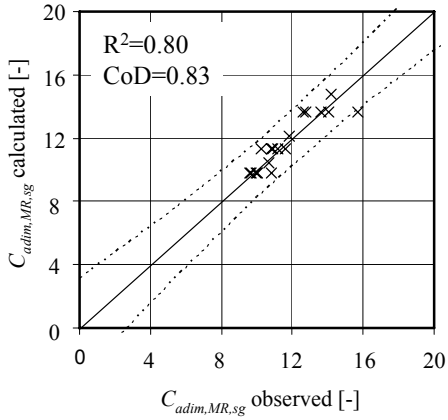

Figure 8: Friction coefficients obtained for the square grooved flow type (Eq. (24)).

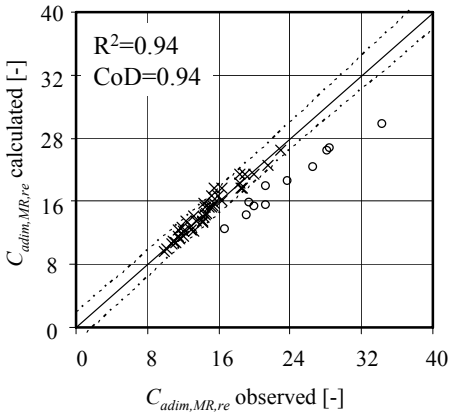

Figure 9: Friction coefficients obtained for the reattachment flow type (Eq. (21) with $\Delta B^* = \Delta B$).

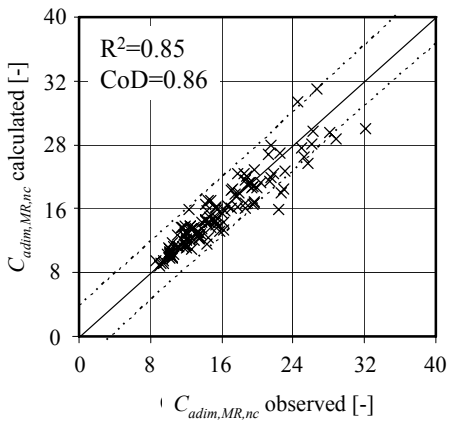

Figure 10: Friction coefficients obtained for the normal recirculating flow type (Eq. (21), (22) and (23)).

The formulas for the reattachment and normal recirculating flow type developed in this section are based on the isolated roughness flow type according Morris (1955). The wall velocity ratio has been chosen $V_w / U = 1$ in order to simplify the formulas and due to a lack of detailed information. This choice has an influence on the drag coefficient of the sharp edged cavity C_d which would be 2.25 or 4 times higher when assuming a ratio of $V_w / U = 2/3$ or $1/2$ ($C_d' = 1.07 \div 1.90$). These C_d' values fit to the drag coefficients proposed by Morris (1972) for rectangular depressions.

The reattachment flow type is similar to the isolated roughness flow type according Morris, for which, very good agreement has been found. The experiments indicated with (o) correspond to low discharge experiments with an aspect ratio of $\Delta B / L_b = 0.1$. As mentioned, the flow may not completely reattach to the side wall but recirculates. Most of these cases are better solved by the normal recirculating flow type formula. For the normal recirculating flow type the agreement is still quite good. The expansion of the flow inside the cavity has to be taken into account by an empirical formula based on the Reynolds number of the flow and the cavity geometry. Additional investigations in a short flume including only a few widenings and at different scales would be interesting to justify or reject this proposition. The adapted, but physically based model for square grooved flows can predict the observed friction coefficients with good agreement for $Re_m > 60'000$. For lower Reynolds numbers, no satisfying mathematical description could be found since only limited data is available. The difficulty to quantify correctly depression-type roughness has already been mentioned by Jiménez (2004).

5 CONCLUSIONS

The experiments conducted in 41 different geometrical configurations showed various two dimensional flow characteristics in the cavities. The overall head-loss of the flow is governed by the existence of different phenomena such as vertical mixing layers, wake-zones, recirculation gyres, coherent structures and skin friction. The macro-rough flow resistance has been described by two different approaches.

From the author's point of view, the description of the macro-roughness flow resistance by a form drag based model seems to be the best. The necessary subdivision in square grooved, reattachment and normal recirculating flow types is physically based and further investigations on a smaller model would make possible the determi-

nation of the drag coefficients of macro-roughness elements other than rectangular cavities.

Further research on C_d coefficients for other roughness geometries and on the flow expansion in normal recirculating flow type could help to consolidate the presented developments and to expand the application range.

REFERENCES

Bathurst, J. C. 1978. Flow resistance of large-scale roughness. Journal of the Hydraulics Division-ASCE, 104(12), 1587–1603.

Baumann, P., and Klaus, I. 2003. Gewässerökologische Auswirkungen des Schwallbetriebes - Ergebnisse einer Literaturstudie. Bundesamt für Umwelt, Wald und Landschaft BUWAL, Bern, Switzerland.

Bousmar, D., and Zech, Y. 1999. Momentum transfer for practical flow computation in compound channels. Journal of Hydraulic Engineering - ASCE, 125(7), 696-706.

Canovaro, F., and Solari, L. 2006. Flow resistance associated to a schematic step-pool pattern. In L. Ferreira, Alves and Cardoso (Eds.), River Flow 2006, Volume 1, pp. 1005–1011; ISBN 0-415-40815-6.

Carlier, M. 1988. Hydraulique générale et appliqué. Eyrolles, Paris, France.

Céréghino R., P. Cugny, Lavandier, P. 2002. Influence of intermittent hydropeaking on the longitudinal zonation patterns of benthic invertebrates in a mountain stream. International Review of Hydrobiology 87(1): 47–60.

Cushman, R. M. 1985. Review of ecological effects of rapidly varying flows downstream of hydroelectric facilities. North American Journal of Fisheries Management, 5: 330-339.

Einstein, H. A. 1934. Der hydraulische oder Profilradius. Schweizerische Bauzeitung, 103(8): 147-150.

Favre, H. 1935. Etude théorique et expérimentale des ondes de translation dans les canaux découverts. Dunod, Paris.

Ferro, V. 2003. Flow resistance in gravel-bed channels with large-scale roughness. Earth Surface Processes and Landforms, 28: 1325-1339.

Giustolisi, O., Savic, D. A. 2006. A Symbolic Data-driven Technique Based on Evolutionary Polynomial Regression. Journal of Hydroinformatics, 8(3), 207–222.

Jiménez, J. 2004. Turbulent Flows over Rough Walls. Annual Review of Fluid Mechanics. 36: 173-196

Lawrence, D. S. L. 1997. Macroscale surface roughness and frictional resistance in overland flow. Earth Surface Processes and Landforms, 22, 365-382.

Leonardi, S., Orlandi, P., Smalley, R. J., Djenidi, L., and Antonia, R. A. 2003. Direct numerical simulation of turbulent channel flow with transverse square bars on one wall. Journal of Fluid Mechanics, 491, 229-238.

Meile, T. 2007. Influence of macro-roughness of walls on steady and unsteady flow in a channel. Ph.D. Thesis N° 3952 de l'Ecole Polytechnique Fédérale de Lausanne and Mitteilung Nr. 36 des Wasserbaulabors der ETH Lausanne (LCH-EPFL); ISSN 1661-1179.

Meile, T., Boillat, J.-L., Schleiss, A. J. 2008. Dämpfende Wirkung von grossmassstäblichen Uferrauheiten auf Schwall und Sunkerscheinungen in Flüssen. Wasser-Wirtschaft 98 (12), 18-24.

Meile, T., Boillat, J.-L., Schleiss, A. J. 2010 (submitted). Water surface oscillations in a channel with axi-symmetric cavities. Journal of Hydraulic Research.

Meyer-Peter, E., and Müller, R. 1948. Formulas for bed-load transport. Report on the 2nd meeting of the IAHSR (today IAHR), Stockholm, Sweden, 39-64.

Morris, H. M. 1955. Flow in Rough Conduits. Transactions of the American Society of Civil Engineers, 120, 373-410.

Pagliara, S., Chiavaccini, P. 2006. Flow Resistance of Rock Chutes with Protruding Boulders. Journal of Hydraulic Engineering - ASCE, 132(6), 545-552.

Rouse, H. 1965. Critical Analysis of Open-Channel Resistance. Journal of Hydraulics Division, 91(HY4), 1-25.

Sieben, J. 2003. Estimation of effective hydraulic roughness in non-uniform flow. XXX IAHR Congress, Thessaloniki, Greece, 17-24.

Stranner, H. 1996. Schwallwellen im Unterwasser von Spitzenkraftwerken und deren Reduktion durch flussbauliche Massnahmen. Schriftenreihe zur Wasserwirtschaft N°20, Technische Universität Graz, Austria.

Wang Z.-H., Melching C. H., Duan X. D., and Yu G. Y. 2009. Ecological and hydraulic studies of step-pool systems, ASCE Journal of Hydraulic Engineering, 134(9): 705-717.

Weichert, R. 2006. Bed Morphology and Stability in Steep Open Channels. Ph.D. Thesis N°16316, ETHZ, Zürich, Switzerland.

Weitbrecht, V. 2004. Influence of dead-water zones on the dispersive mass transport in rivers, Dissertationsreihe am Institut für Hydromechanik der Universität Karlsruhe (TH) Heft 2004/1, Karlsruhe, Germany.

Yen, B. C. 2002. Open Channel Flow Resistance. Journal of Hydraulic Engineering - ASCE, 128(1), 20-39.